Volume 9, Number 2 (April 2016) p. 153 - 191 • ISSN 1983-4195
http://dx.doi.org/10.1590/S1983-41952016000200002

REVISTA IBRACON DE ESTRUTURAS E MATERIAIS
IBRACON STRUCTURES AND MATERIALS JOURNAL

Numerical analysis of steel-fiber-reinforced concrete beams using damage mechanics

Análise numérica de vigas de concreto com fibras de aço utilizando mecânica do dano

W. M. PEREIRA JUNIOR [a]
w.junioreng@gmail.com

D. L. ARAÚJO [b]
araujodl@terra.com.br

J. J. C. PITUBA [b]
jjpituba@yahoo.com.br

Abstract

This work deals with numerical modeling of the mechanical behavior of steel-fiber-reinforced concrete beams using a constitutive model based on damage mechanics. Initially, the formulation of the damage model is presented. The concrete is assumed to be an initial elastic isotropic medium presenting anisotropy, permanent strains, and bimodularity induced by damage evolution. In order to take into account the contribution of the steel fiber to the mechanical behavior of the media, a homogenization procedure is employed. Finally, numerical analyses of steel-fiber-reinforced concrete beams submitted to bending loading are performed in order to show the good performance of the model and its potential.

Keywords: damage mechanics, steel-fiber-reinforced concrete beams, constitutive model, concrete.

Resumo

O artigo trata de uma contribuição à modelagem numérica do comportamento mecânico de vigas de concreto armado reforçado com fibras de aço utilizando modelos constitutivos baseados na Mecânica do Dano. O mesmo apresenta a formulação de um modelo de Dano proposto que admite o concreto como material inicialmente isótropo e elástico, mas com a evolução do processo de danificação, exibe deformações plásticas, anisotropia e bimodularidade induzidas pelo dano. A incorporação das fibras na modelagem é efetuada por meio de um procedimento de homogeneização. Por fim, análises numéricas de vigas de concreto armado reforçado com fibras de aço sujeitas à flexão são realizadas com o objetivo de avaliar a aplicabilidade da modelagem proposta.

Palavras-chave: mecânica do dano, vigas de concreto reforçado com fibras de aço, modelo constitutivo, concreto.

[a] *Pontifícia Universidade Católica de Goías, Goiânia, GO, Brasil;*
[b] *Universidade Federal de Goías, Goiânia, GO, Brasil.*

Received: 23 May 2015 • Accepted: 28 Sep 2015 • Available Online 21 Mar 2016

1. Introduction

Every mechanical system submitted to static, dynamic, or thermal loads presents a response. However, complex analyses must be performed to obtain the mechanical response because the mechanical system is composed of several structural elements that evidence different mechanical behaviors. Some studies have reported the use of different constitutive models for analysis of mechanical concrete systems, such as references [1], [2], and [3].

In the context of numerical theories used in computational mechanics, Continuum Damage Mechanics (CDM) deserves a mention, because it shows reliable numerical responses for mechanical systems composed of complex materials like concrete. An important work was developed by La Borderie [4], who proposed a homogenization rule with a damage model for fiber-reinforced concrete in order to obtain the updated stress in the composite matrix.

On the other hand, Li and Li [5] studied concrete damage models applied to the analysis of tensioned fibers. In their work, the concrete was treated as a medium that shows hardening behavior for increasing strain. The results are satisfactory when compared to experimental ones. The same observation is valid for the work developed by Lee and Liang [6], who applied CDM to fiber-reinforced cellular concrete.

Moreover, Hameed *et al.* [7] used damage mechanics to model steel-fiber-reinforced concrete beams, obtaining satisfactory results when compared to experimental tests. Pasa [8] also evaluated the mechanical behavior of steel-fiber-reinforced concrete using the finite element method with smeared crack models.

According to Guello [9], the nonlinear behavior of the concrete, which takes place even at low stress levels, is influenced by nucleation and propagation of microcracks during the loading process. Thus, the importance of a reliable cracking model can be seen. However, in the context of improved materials for structural application, nowadays, steel-fiber-reinforced concrete is largely used, which reduces the tensile brittle behavior of concrete, leading to a better strain capacity due to the clipping effect of the cracks provided by fibers.

According to reference [18], the effect of the addition of steel fibers on the flexural strength of concrete and mortar is more evident with regard to the tensile behavior than the compression strength. This paper intends to present a proposal for modeling the mechanical behavior of fiber-reinforced concrete using the damage model proposed by Pituba and Fernandes [3], which has already been tested in conventional concrete structures. The one-dimensional version of this proposed modeling is presented and applied to the analysis of fiber-reinforced concrete beams in order to mark out a discussion about the viability and employment restrictions in simplified numerical analyses in the context of structural engineering.

2. Computational modeling

2.1 Modeling of reinforcement

In this paper, a one-dimensional model has been used to describe the mechanical behavior of reinforcement bars, which contribute only to the axial strength of the structure. The reinforcement transversal section is transformed into a layer located according to its center of gravity (see Figure 1). A bilinear elastoplastic model is used to represent the tension and compression behavior of reinforcement bars.

2.2 Damage model for concrete

In this paper, it can be assumed that the concrete belongs to the category of materials that can be considered as initially isotropic and unimodular, showing different behaviors in tension and compression regimes. Also, transverse isotropic behavior is shown when the medium presents a damage process. Moreover, the model respects the principle of energy equivalence between the damaged real medium and the equivalent continuum medium established in the CDM and presented by Pituba and Fernandes [3]. The damage model proposed in [3] is briefly described. Initially, for dominant tension states, a damage tensor can be written as:

$$\boldsymbol{D_T} = f_1(D_1, D_4, D_5)(\boldsymbol{A} \otimes \boldsymbol{A}) + 2\, f_2(D_4, D_5)\, [(\boldsymbol{A} \underline{\otimes} \boldsymbol{I} + \boldsymbol{I} \underline{\otimes} \boldsymbol{A}) - (\boldsymbol{A} \otimes \boldsymbol{A})] \quad (1)$$

where $f_1(D_1, D_4, D_5) = D_1 - 2\, f_2(D_4, D_5)$ and $f_2(D_4, D_5) = 1 - (1-D_4)(1-D_5)$.

The variable D1 represents the damage in the direction orthogonal to the transverse isotropy local plane of the material, while D4 is representative of the damage due to the sliding movement between the crack faces. The third damage variable, D5, is only activated if a previous compression state accompanied by damage has occurred. The tensor I is the second-order identity tensor, and the tensor A is formed by the dyadic product of the unit vector perpendicular to the transverse isotropy plane for itself. Those products are given in [3].

Figure 1 – Finite element applied to Pituba's computer code (10)

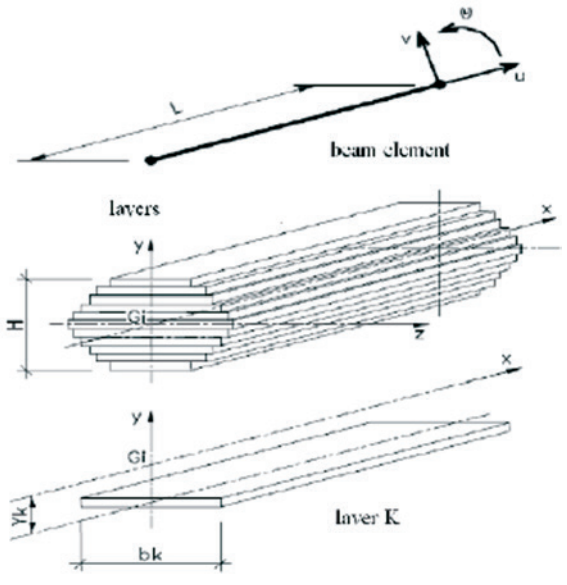

For dominant compression states, another damage tensor is proposed:

$$\boldsymbol{D_C} = f_1(D_2,D_4,D_5)\,(\boldsymbol{A}\otimes\boldsymbol{A}) + f_2(D_3)\,[(\boldsymbol{I}\overline{\otimes}\boldsymbol{I}) - (\boldsymbol{A}\otimes\boldsymbol{A})] + 2f_3(D_4,D_5)\,[(\boldsymbol{A}\underline{\otimes}\boldsymbol{I} + \boldsymbol{I}\underline{\otimes}\boldsymbol{A}) - (\boldsymbol{A}\otimes\boldsymbol{A})] \quad (2)$$

where $f_1(D_2, D_4, D_5) = D_2 - 2\,f_3(D_4, D_5)$, $f_2(D_3) = D_3$ and $f_3(D_4, D_5) = 1 - (1-D_4)\,(1-D_5)$.

Note that the compression damage tensor introduces two additional scalar variables in its composition: D2 and D3. The variable D2 (damage perpendicular to the transverse isotropy local plane) reduces the Young's modulus in that direction and, in conjunction with D3 (which represents the damage in the transverse isotropy plane), degrades the Poisson's ratio throughout the planes perpendicular to the transverse isotropy plane.

Finally, the constitutive tensor is written as:

$$\boldsymbol{E_T} = \lambda_{11}[I\otimes I] + 2\mu_1[I\underline{\otimes}I] - \lambda^{+}_{22}(D_1,D_4,D_5)\,[A\otimes A] - \lambda^{+}_{12}(D_1)\,[\boldsymbol{A\ \ I + I\ \ A}] - \mu_2(D_4,D_5)\,[A\underline{\otimes}I + I\underline{\otimes}A] \quad (3)$$

$$E_C = \lambda_{11}[I\otimes I] + 2\mu_1[I\underline{\otimes}I] - \lambda^{-}_{22}(D_2,D_3,D_4,D_5)\,[A\otimes A] - \lambda^{-}_{12}(D_2,D_3)\,[\boldsymbol{A\ \ I + I\ \ A}] - \lambda^{-}_{11}(D_3)\,[\boldsymbol{I\ \ I}] - \frac{(12)\,\nu_0}{\nu_0}\lambda^{-}_{113}(D)\,[I\bar{\otimes}I] - \mu_2(D_4,D_5)\,[A\underline{\otimes}I + I\underline{\otimes}A] \quad (4)$$

where $\lambda_{11} = \sigma_0$ and $\mu_1 = \mu_0$. The remaining parameters will exist only for no-null damage, evidencing the anisotropy and bimodularity induced by the damage process. Those parameters are given by:

$$\lambda^{+}_{22}(D_1,D_4,D_5) = (\lambda_0 + 2\mu_0)(2D_1 - D_1^2) - 2\lambda^{+}_{12}(D_1) - 2\mu_2(D_4,D_5)$$
$$\lambda^{+}_{12}(D_1) = \lambda_0 D_1;\ \ \mu_2(D_4,D_5) = 2\mu_0[1-(1-D_4)^2(1-D_5)^2]$$
$$+\frac{(\nu_0 - 1)}{\nu_0}\lambda^{-}_{11}(D_3) - 2\mu_2(D_4,D_5) \quad (5)$$

$$\lambda^{-}_{12}(D_2,D_3) = \lambda_0[(1-D_3)^2 - (1-D_2)(1-D_3)] \quad (6)$$

$$\lambda^{-}_{11}(D_3) = \lambda_0(2D_3 - D_3^2);$$
$$\mu_2(D_4,D_5) = 2\mu_0[1-(1-D_4)^2(1-D_5)^2] \quad (7)$$

The constitutive model includes two damage tensors in order to take into account the bimodularity induced by damage in the concrete behavior. Therefore, a criterion defining the tension and compression dominant states is necessary to indicate what damage tensor should be used. Besides, there are two criteria dealing with the beginning and evolution of the damage process. More details can be found in Pituba and Fernandes [3].

The one-dimensional version of the damage model has been implemented in a finite element code for bar structures analysis with finite layered elements in order to model the reinforced concrete framed structures (Figure 1). In the transversal section, a certain layer can contain steel and concrete. A perfect adherence between materials is adopted and an equivalent elasticity modulus and inelastic strain are defined for each layer by using the homogenization rule (see reference [3]).

The model proposed in reference [3] does not take into account plastic strains that arise when unloading situations take place. Thus, if plastic strains are not negligible, they should be considered for reliable modeling in unloading situations.

In fact, the inelastic strains and damage occur simultaneously. According to La Borderie [4], microcracking and the existence of voids in the material are responsible for those phenomena. The microvoids are a cause of inelastic strains because they do not permit the full closure of microcracks in the unloading processes. On the other hand, the surfaces of the microcracks are irregular, and this is another reason for the difficulty in achieving their total closure.

Taking into account just the uniaxial cases, the formulation of the proposed model is then extended to incorporate permanent strains, which are assumed to appear after the damage has been activated. Assuming, for simplicity, that the permanent strains are exclusively composed of volumetric strains, as has already been considered in other work [11], and taking into account the unilateral effect, the evolution law for the permanent strains is:

$$\varepsilon^{P} = \frac{\partial g_T}{\partial \sigma} D_T + \frac{\partial g_C}{\partial \sigma} D_C \quad (8)$$

where g_T and g_C are inelastic potentials.

For simplicity, it is assumed that the plastic strains are exclusively composed of volumetric strains [12]. The potentials can be expressed by:

$$g_T = \beta_T(D_T)\,I_1 \quad (9)$$

$$g_C = \beta_C(D_C)\,I_1 \quad (10)$$

where the damage functions $\beta_T(D_T)$ and $\beta_C(D_C)$ are material parameters. In order to apply the damage model to concrete, the following functions are adopted:

$$\beta_T(D_T) = \frac{\beta_1}{(1-D_1)^2} \quad (11)$$

$$\beta_C(D_C) = \frac{\beta_2}{(1-D_2)^2} \quad (12)$$

where I_1 is the first invariant of the stress tensor. Therefore, Eq. 8 is given by:

$$\varepsilon^P = \beta_T(D_T) I_1 D_T + \beta_C(D_C) I_1 D_C \quad (13)$$

Finally, the evolution law for plastic strains ε^P, taking into account the unilateral effect, is:

$$\varepsilon^P = \left(\frac{\beta_1}{(1-D_1)^2} D_1 + \frac{\beta_2}{(1-D_2)^2} D_2 \right) I_1 \quad (14)$$

Observe that β_T T and β_C C are parameters that are directly related to the evolution of permanent strains induced by damage in tension and in compression, respectively. When these parameters are null, the constitutive model originally proposed in reference [3] is recovered. It is important to note that uniaxial tests in tension and compression with loading and unloading are necessary for the identification of parameters β_T T and β_C.

On the other hand, considering Direction 1 as the longitudinal direction of the finite element, the formulation previously presented is simplified and described as follows:

$$E(\varepsilon) = \begin{cases} E_C \; seg(\varepsilon, D_T, D_C) < 0 \\ E_T \; seg(\varepsilon, D_T, D_C) > 0 \end{cases} \quad (15)$$

$$E_T = E(1-D_1)^2(1-D_2)^2 \quad (16)$$

$$E_C = E(1-D_2)^2 \quad (17)$$

The complementary elastic energies of the damaged medium in tension- and compression-dominant states, respectively, as well as the variables associated with damage variables, are now expressed by:

$$W^*_{e+} = \frac{\sigma_{11}^2}{2E(1-D_1)^2(1-D_2)^2} \quad (18)$$

$$W^*_{e-} = \frac{\sigma_{11}^2}{2E(1-D_2)^2} \quad (19)$$

$$Y_T = \frac{\partial W^*_{e+}}{\partial D_1} = Y_1 \quad (20)$$

$$Y_C = \frac{\partial W^*_{e-}}{\partial D_2} = Y_2 \quad (21)$$

$$Y_1 = \frac{\sigma_{11}^2}{2E(1-D_1)^3(1-D_2)^2}; Y_2 = \frac{\sigma_{11}^2}{E(1-D_2)^3} \quad (22)$$

More details can be found in Pituba and Fernandes [3]. Figure 1 shows the finite element used in this paper to perform the numerical analyses.

2.3 Homogenization model for steel fibers in concrete

The mechanical behavior of the steel-fiber-reinforced concrete structures submitted to loading and unloading processes depends on the interaction between fibers and matrix. In this paper, the homogenization procedure proposed by La Borderie [4] is used. The constitutive relationship of the steel-fiber-reinforced concrete in the dominant tension regime is presented in Figure 2, which is obtained from the fiber pullout test. The following parameters can be obtained from this test: peak stress (σ_{pic}), initial yield stress (σ_s), and ultimate strain (ε_{rupt}).

Figure 2 – Model of tensile behavior in concrete with fibers proposed by La Borderie (4)

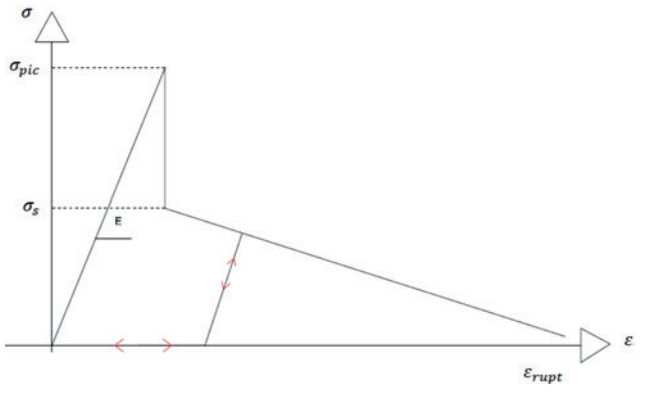

Table 1 – Features of the steel fibers used by Velasco (13)

Analysed property	Value
Specific weight (kg/m³)	7800
Length (mm)	35
Diameter (mm)	0.54
Aspect ratio (l/d)	65
Modulus of elasticity (GPa)	202
Tensile strength (MPa)	1342

On the other hand, via the Voigt kinematic homogenization method, La Borderie [4] proposed the following expression for calculating the homogenized stress of the composite:

$$\sigma_{CRFA} = (1-C)\sigma_m + C\sigma_f \quad (23)$$

where:
σ_{CRFA} : homogenized stress;
C : volumetric fraction of the steel fibers;
σ_m : concrete matrix stress;
σ_f : interfacial fiber–matrix stress;
It can be observed that a simplifying assumption has been introduced: the strain of the fiber and the matrix is considered the same. Furthermore, the random fiber orientation is not taken into account in the proposed homogenization.

3. Numerical examples

3.1 Modeling of Velasco´s tests [13]

The first numerical example deals with steel-fiber-reinforced concrete prisms submitted to a bending moment and tested by Velasco [13]. The steel fibers are named A to I in accordance with NBR 15530:2007 [14]. Table 1 shows the main characteristics of the steel fibers.
The concrete mixtures used in Velasco's tests [14] were previously studied by Lopes [15]. MCWSF concrete matrix (see reference [13]) was chosen for the numerical modeling as well as steel-fiber-reinforced concretes with fiber contents of 1.0% (MCWSFA10), 1.5% (MCWSFA15), and 2.0% (MCWSFA20). Table 2 shows the characteristics of the concrete mixtures.

3.1.1 Parametric identification of the Damage Model

Firstly, it is necessary obtain the values of the damage model parameters of the concrete matrix in order to model the behavior of the steel-fiber-reinforced concrete. For this purpose, the MCWSF concrete matrix is taken (Table 2). These parameters were obtained from the uniaxial compression and tension tests performed by Velasco [13]. The stress–strain curve for tension was obtained from 100 × 100 × 400 mm prismatic specimens molded in the horizontal direction, whereas the stress–strain curve for compression was obtained from tests on cylindrical specimens [19]. From an inverse analysis of these tests, the values of the damage parameters for the concrete matrix were found and are listed in Table 3.
Soon after, these damage parameters were used to model 100 × 100 × 400 mm prismatic specimens with a span of 300 mm and were submitted to bending moments. Nineteen finite elements with ten layers each were used for modeling the prismatic specimen.

Table 2 – Mechanical properties of concrete studied by Lopes (15)

Concrete	Nomenclature	f_{cm} (MPa)	Modulus of elasticity (GPa)	Poisson ratio (ν)	Fiber percentage (%)
1	MCWSF	55.1	35.7	0.17	0.00
2	MCWSFA10	61.7	34.8	0.19	1.00
3	MCWSFA15	70.0	37.4	0.19	1.50
4	MCWSFA20	72.4	37.7	0.21	2.00

Table 3 – Damage parameters identified for concrete without fibers submitted to axial compression and tensile

Damage variable for compression		Damage variable for tensile	
A_2	0.7	A_1	15
B_2 (Mpa^{-1})	2.5	B_1 (Mpa^{-1})	1200
YO_2 (Mpa)	0.004945	YO_1 (Mpa)	0.000086
β_2	0.000300	β_1	0.000025

Table 4 – Damage parameters and modulus of elasticity identified for concrete with 0.0% fibers from four-point flexural test on prismatic specimens of 100 mm × 100 mm × 400 mm

Parameters	Tensile	Compression	$F_{pico,\ num}$ / $F_{pico,\ exp}$
E Mpa	41000	41000	0.0860%
A	15	0.7	0.0860%
B (Mpa^{-1})	1030	2.5	0.0860%
YO (Mpa)	0.00085	0.04945	0.0860%
B	0.00000045	0.0003	0.0860%

Table 5 – Model parameters of homogenization of La Borderie (4) for concrete with 1.0, 1.5, and 2.0% steel fibers – Example I

Fiber volume	$F_{pico,\ num}$ (kN)	Peak stress – σ_{pic} (MPa)	Yield stress – σ_s (MPa)	Strain fracture – ε_{rupt} (m/m)	$F_{pico,\ num}$ / $F_{pico,\ exp}$
1.00%	38.20	530.00	477.00	0.0200	0.0460%
1.50%	58.00	570.00	513.00	0.0220	0.9600%
2.00%	62.80	460.00	414.00	0.0220	1.0800%

The load–displacement curve in the middle of the span obtained from the damage model was compared with result of the experimental test. This comparison showed that the numerical response obtained from the damage model was not satisfactory and, for this reason, new values for the damage model parameters in tension were determined (Table 4). A strong sensibility of the tension

Figure 3 – Comparison of load curve versus displacement in the numerical and experimental middle-span of Velasco (13) for the four-point flexural test with concrete with 0.0% fibers

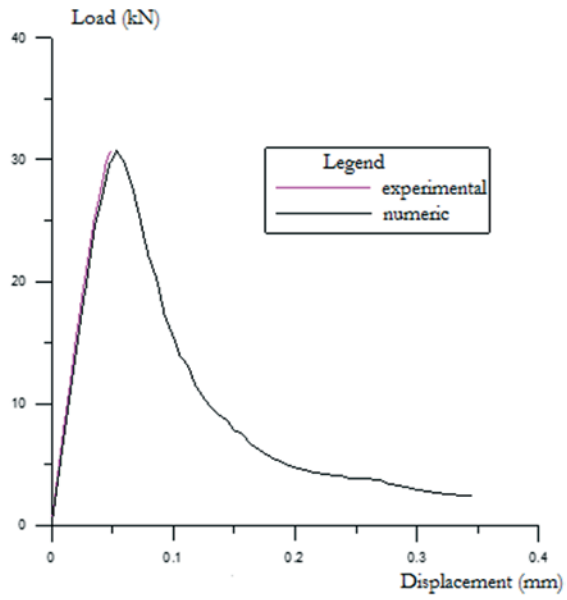

Figure 4 – Comparison of load curve versus displacement in the numerical and experimental middle-span for the four-point flexural test with concrete with 1.0% fibers

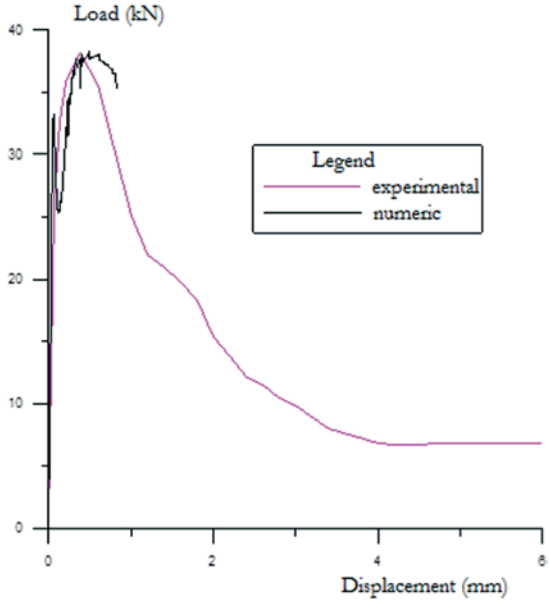

damage parameters was evidenced after convergence problems arose in peak loadings due to the high level of damage processes in tensioned concrete layers. This evidences damage localization processes in the middle of the span that the damage model is not capable of describing. The final result for the concrete without fibers is illustrated in Figure 3.

In sequence, the homogenization model parameters proposed by La Borderie [14] were obtained for the concrete with steel fibers. An inverse analysis from prismatic specimens submitted to four bending points, with the same dimensions of the prismatic specimens without fibers, was used for the parametric identification of the SFRC [13]. The numerical and experimental responses are presented in Figures 4 to 6, where the numerical responses are considered satisfactory. The difference between numerical and experimental peak loads is smaller than 1%. The values of the homogenization model parameters are listed in Table 5. All analyses related to damage processes are presented in Section 3.2.1.

3.1.2 Analyses of damage process

In order to analyze the damage distribution in the prismatic specimens with steel-fiber-reinforced concrete, the tension damage values near to peak loading are shown in Figure 7a. It can be observed that there is a high-level damage process at the bottom and middle span of the prism and a vanishing process of the damage is evidenced towards the support of the prism.

For the concrete with a steel fiber content of 1.5%, the numerical modeling shows up to 1.05 mm of displacement at the middle of the span near to peak loading. The damage process in the prism is illustrated in Figure 7b. For the concrete with a steel fiber content of 2.0%, the damage distribution near to peak loading is shown in Figure 7c.

Figure 8 and Table 6 show results of the effect of the steel fiber in the system for a load level of 30 kN. From this figure and the table it is possible to note that the specimen with the highest fiber content showed lower damage at the same loading level, which evidences the crack clipping by steel fibers, which leads to increased tensile strength of the concrete specimen.

3.2 *Modeling of Lopes´s tests [15]*

The second numerical example deals with the analysis of a beam tested by Lopes [15]. Steel fibers A to I were used and their characteristics are given in Table 7. Table 8 shows the mechanical properties of the concrete used to make up the beam analyzed in this section.

3.2.1 Parametric identification of the damage model

The damage model parameters in tension for concrete without fibers were obtained from inverse analysis of prismatic specimens of 100 × 100 × 400 mm (Figure 9) with a span of 300 mm. These specimens were submitted to four-point bending tests. On the other hand, the same parameters were adopted for compression as for the previous numerical example (Table 9). The comparison between experimental and numerical responses is shown in reference [16]. A tolerance factor of 5% between experimental and numerical peak loads was adopted. The elasticity modulus for the concrete obtained in tests was used here.

Figure 5 – Comparison of load curve versus displacement in the numerical and experimental middle-span for the four-point flexural test with concrete with 1.5% fibers

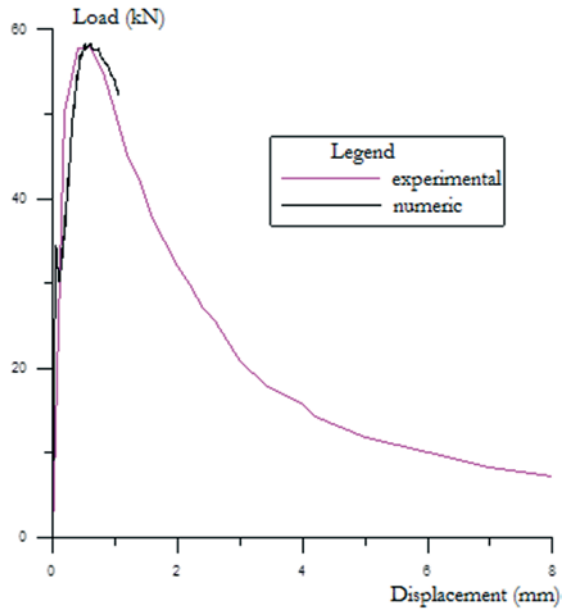

Figure 6 – Comparison of load curve versus displacement in the numerical and experimental middle-span for the four-point flexural test with concrete with 2.0% fibers

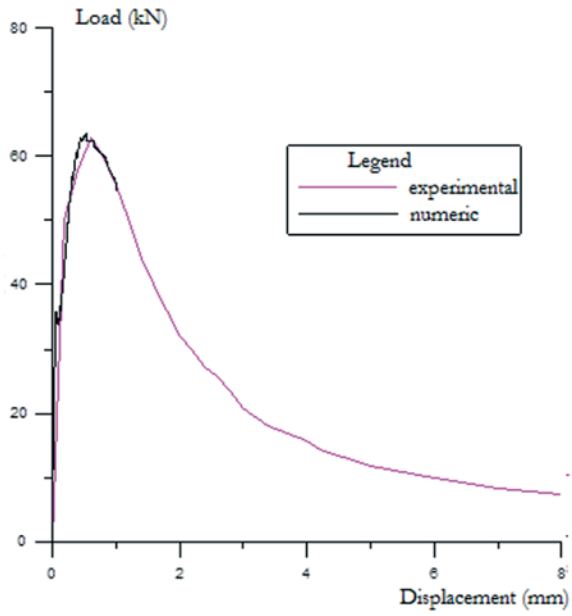

Figure 7 – Graphical representation of tensile damage (D_t) in concrete prismatic specimens

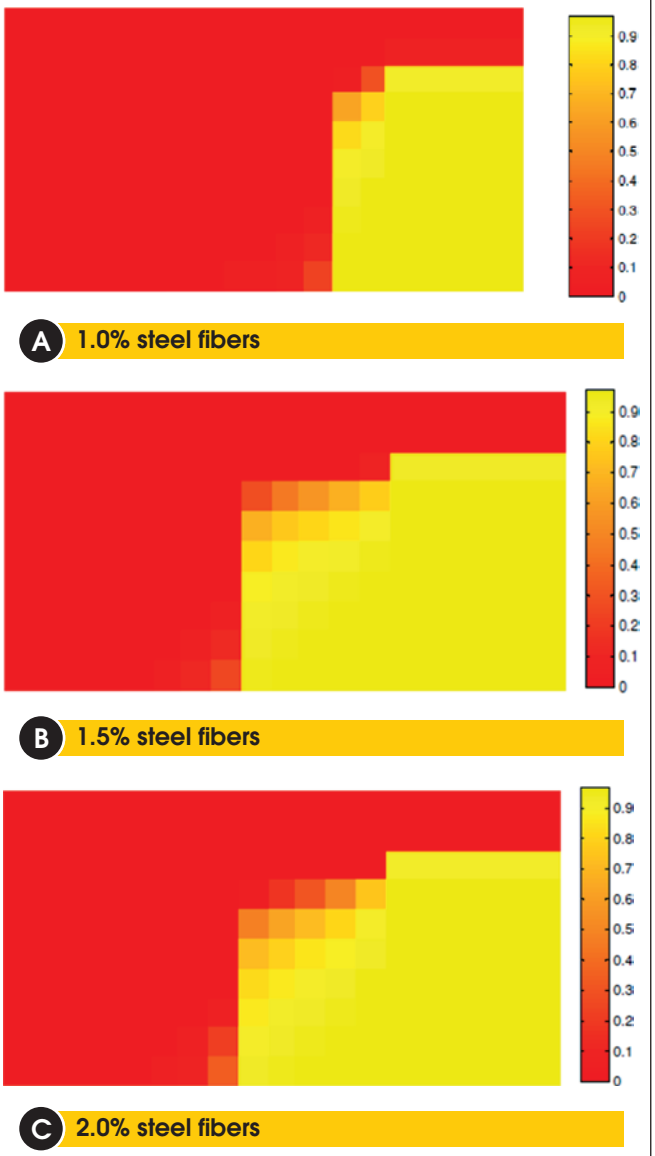

Soon after, the parameters of the homogenization model proposed by La Borderie [4] for concrete with 2% steel fiber content were determined by inverse analyses of the prismatic specimens tested by Lopes [15]. In this case, the damage model parameters for plain concrete were kept constant. Table 10 lists the values of the homogenization model parameters.

Table 6 – Damage analyses for tension in function of fiber percentage

Fiber percentage	Damaged element	Damage in the element
1.00%	19	0.2563
1.50%	19	0.1184
2.00%	19	0.1179
1,00E-02	1,00E-02	0

Figure 8 – Evolution of damage in the 1° tensileed layer in function of the percentage of fibers in the load of 30 kN

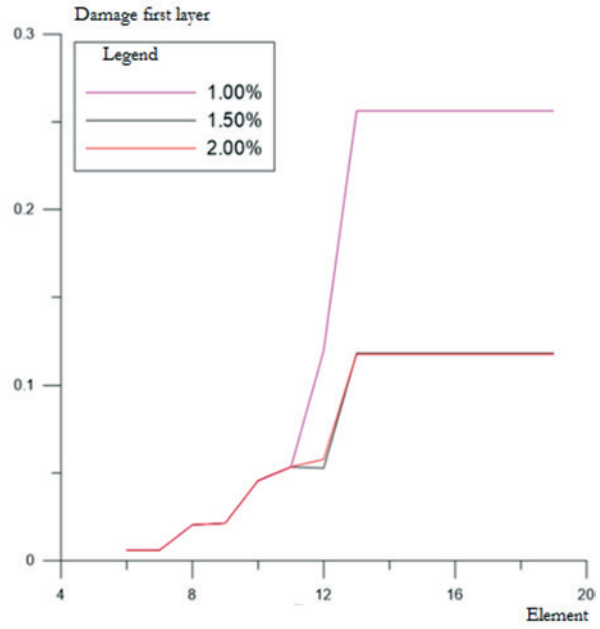

3.2.2 Modeling of beam test

The geometry of the beam analyzed in this example, as well as the bar reinforcement detail, is shown in Figure 10. This beam was made of concrete with a steel fiber content of 2% and was submitted to bending due to two loads applied at two points 100 cm apart from each other.

Due to beam symmetry, only half of the beam was modeled, using 50 finite elements. The cross-section was divided into 24 layers, as shown in Figure 11. The longitudinal reinforcement properties used in the modeling are shown in Table 11. The parameters of the damage model and the homogenization model are the same as those shown in the previous item because the concrete of the beam is the same. Tables 9 and 10 list these parameters.

The comparison between numerical and experimental results is presented in Figure 12. A good approximation can be observed in the initial loading, while there is a divergence between the curves for loading near to structural collapse. This behavior is due to fracture nucleation in the collapse regime, where the damage model does not present an efficient response to damage localization.

Table 7 – Steel fiber properties used by Lopes (15)

Analysed property	Value
Modulus of elasticity (GPa)	200
Tensile strength (MPa)	1150
Specific weight (kg/m³)	7850
Length (mm)	35
Diameter (mm)	0.55
Aspect ratio (l/d)	64

Table 8 – Mechanical properties of concrete obtained by Lopes (15) and used in numerical modeling

Concrete	Nomenclature	f_{cm} (MPa)	Modulus of elasticity (GPa)	Poisson ratio (υ)	Fiber percentage (%)
1	F0V5SPrx1	59.06	34.91	0.20	0.00
2	FAb2V5SPg1	64.22	30.19	0.22	2.00

Figure 9 – Four-point flexure test used to identify the fiber variables

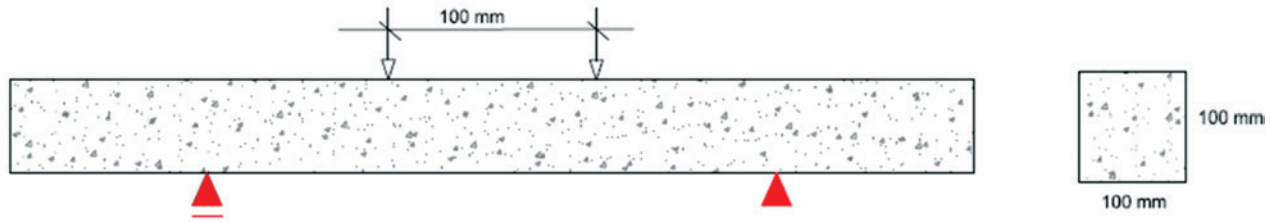

Table 9 – Damage parameters and elastic modulus of concrete without fibers identified from the four-point flexural tests on prismatic specimens of 100 mm × 100 mm × 400 mm

Parameters	Tension	Compression	$F_{pico, num}$ (kN)	$F_{pico, num} / F_{pico, exp}$
E (MPa)	34910	34910	25.746	2.52%
A	15	0.7	25.746	2.52%
B (Mpa^{-1})	1290	2.5	25.746	2.52%
YO (Mpa)	0.000086	0.004945	25.746	2.52%
β	0.00000045	0.0003	25.746	2.52%

Table 10 – Model parameters for homogenization of La Borderier (4) for concrete with 2.0% fibers – Example II

Fiber volume	$F_{pico, num}$ (kN)	Peak stress – σ_{pic} (MPa)	Yield stress – σ_s (MPa)	Strain fracture – ε_{rupt} (m/m)	$F_{pico, num} / F_{pico, exp}$
2.00%	64.49	525.00	420.00	0.0250	0.2444%

Therefore, the analysis of this beam is limited to service loading, which is defined in this paper as a loading lower than 40% of the ultimate load.

This load level was chosen due to the fact that the Brazilian structures are designed in the Ultimate Limit State [NBR 6118, 2014]. In the context of a normal combination of loadings, the loads are increased by a coefficient equal to 1.4 and the material's strength is decreased by coefficients equal to 1.4 for concrete and 1.15 for steel reinforcement. If the collapse load of the beam is divided by the product of these coefficients in order to obtain the structural service loading, a value of 44% of the collapse load is obtained. This situation corresponds, approximately, to the rare combination for the Service Limit State established by the Brazilian Standards [NBR 6118, 2014]. A value of 40% of the collapse load was adopted because in the service state only 40 to 70% of the live load is acting on the structures. Then, the service load of the beam tested can be estimated as 68 kN, and a displacement of 3.297 mm in the middle span was obtained from this load. The displacement obtained from the numerical simulation for this load was 2.695 mm, which represents an error of 18% in the evaluation of the vertical

Table 11 – Steel data used in the beam modeling tested by Lopes (15)

Fiber percentage	Damaged element
Modulus of elasticity (MPa)	210000
Yield stress (MPa)	500
Ultimate stress (MPa)	550
Specific weight (kg/m^3)	7850
Failure strain (%)	1.000

Figure 10 – Beam numerically tested based on Lopes (15) geometry

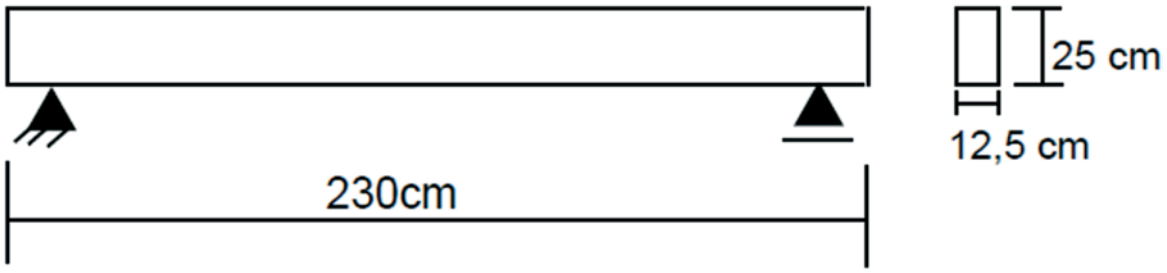

A Geometry of the beam tested by Lopes (15)

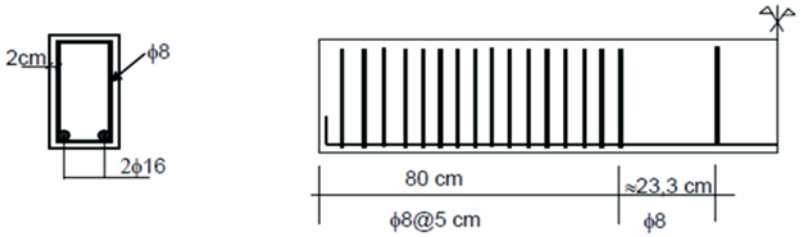

B Beam reinforcement tested by Lopes (15)

displacement of the beam. On the other hand, the displacement obtained using the NBR 6118 [2014] procedure is 3.69 mm. This value is 12% higher than the displacement observed in the test for loading of 68 kN.

The tension damage distribution in the beam near to service loading is shown in Figure 13. It can be noted that the increasing load also leads to increasing damage and dissipates more and more along the beam. Besides, it can be noted that the damage variable already presents high values in the service load state, and in the more tensioned regions it approaches 0.9. This is observed more clearly in Figure 19, which shows the evolution of damage in the first tensioned layer in the middle span of the beam.

Figure 15 shows a general view of the tension damage distribution in the beam at the load of 85.8 kN, which evidences a cracking concentration in the pure flexure region. This behavior is consistent with the cracking pattern observed in the experimental test. On

Figure 11 – Schematic representation of the cross-section of the beam tested by Lopes (15)

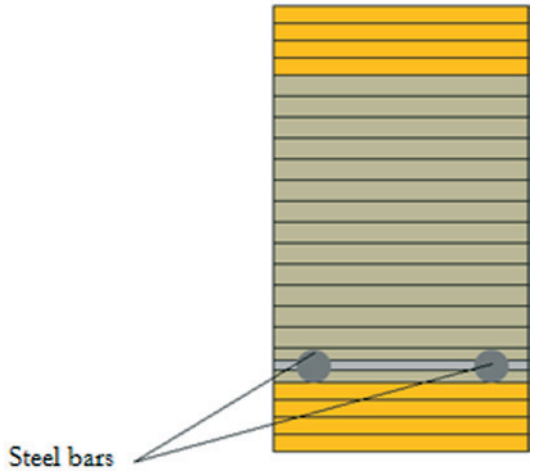

Figure 12 – Chart stress versus displacement of the beam middle-span tested by Lopes (15)

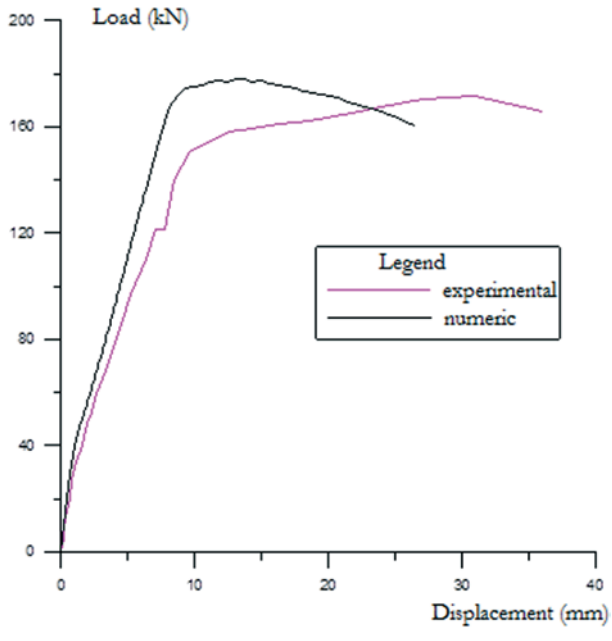

the other hand, because the damage model does not consider the shear contribution, the cracking in the combined shear and flexure region is not well represented by the numerical modeling.

3.3 Modeling of Oliveira´s Tests [17]

The third numerical example deals with the analysis of a beam tested by Oliveira [17]. Steel fibers A to I were used and their characteristics are given in Table 12. Table 13 lists the mechanical properties of the concrete.

3.3.1 Parametric identification of the damage model

Prismatic specimens with different sizes were tested by Oliveira [17] to evaluate the load–displacement curve. The prismatic specimens chosen for numerical analysis in this paper had dimensions of 150 × 150 × 500 mm (span of 400 mm), 100 × 100 × 400 m (span of 300 mm), and 200 × 200 × 800 m (span of 600 mm).
Prismatic specimens with sizes of 150 × 150 × 500 mm and a fiber content of 1.25% were used to identify the damage parameters. This specimen corresponds to the characterization of the concrete of the V9 beam tested by Oliveira [17]. Tables 14 and 15 show the parameter values obtained from the damage model. These parameters were kept constant during the numerical analyses and only the parameters related to the homogenization model were changed. Figure 16 shows the comparison between numerical and experimental responses for the prismatic specimens. The error between the numerical and experimental peak loads was 1.24%. It is important to note that the damage model is not capable of representing the mechanical behavior of the beam when dealing with a high level of displacement due to damage localization.
For the V8 beam with a fiber content of 0.75%, the prismatic specimen of 150 × 150 × 500 mm tested by Oliveira was used again [17]. The parameter values obtained for the homogenization model are presented in Table 16 and the numerical and experimental curves for the prismatic specimen are presented in Figure 23.
For the V7 beam with a fiber content of 0.50%, the three sizes of prismatic specimens tested by Oliveira were analyzed [17]. The parameter values for the homogenization model are presented in Table 17. Note that in this table the parameters are dependent on the specimen size. Figure 18 shows the numerical and experimental responses for the three sizes of the prismatic specimens with fiber contents of 0.50%. It can be clearly observed that the damage model is dependent on the specimen size.

3.3.2 Modeling of the beam tests

Oliveira [17] also performed experimental tests on nine beams in order to determine the influence of steel fibers on the minimum reinforcement of the reinforced concrete beams. Figure 19 shows the geometric characteristics of the beam tested by Oliveira [17]. For the numerical modeling of this beam, 50 finite elements were used and the cross-section was divided into 24 layers, as shown in Figure 11. The properties of reinforcement used in the modeling are shown in Table 18.

Figure 13 – Tensile damage evaluation (D_i) of beam V2 of reinforced concrete with fibers

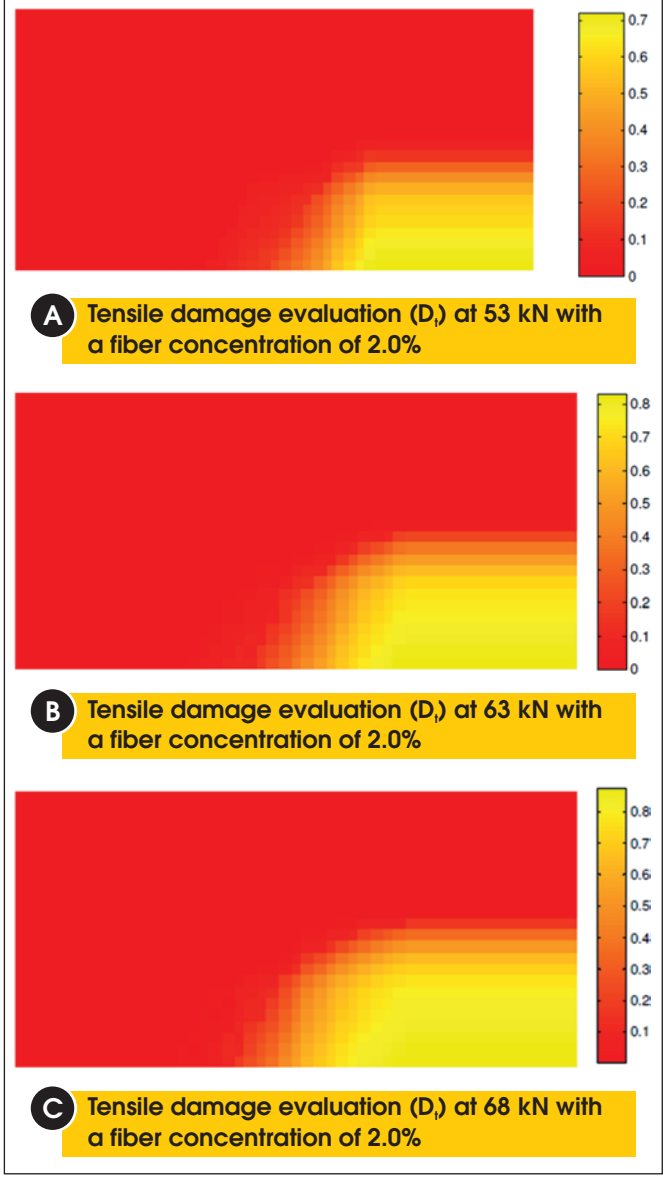

Figure 14 – Damage evolution in the 1° tensioned layer of the beam tested by Lopes (15)

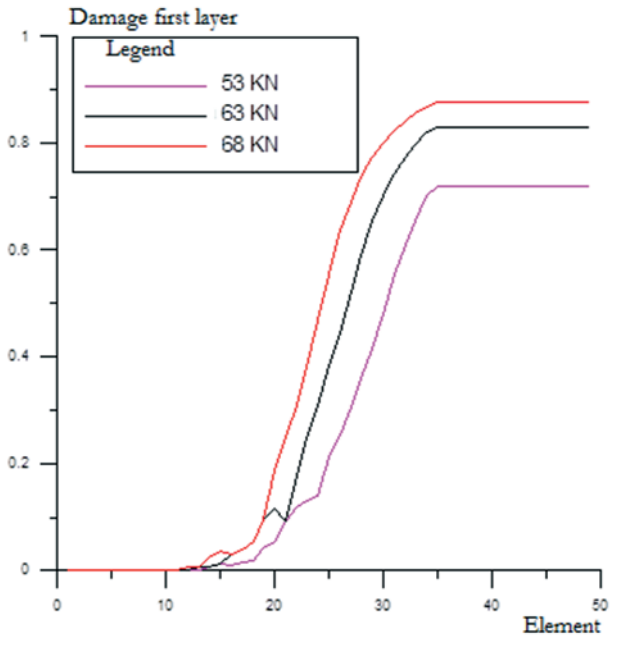

Figure 15 – Comparison of cracking parameters with 85.80 kN load for numerical and experimental values

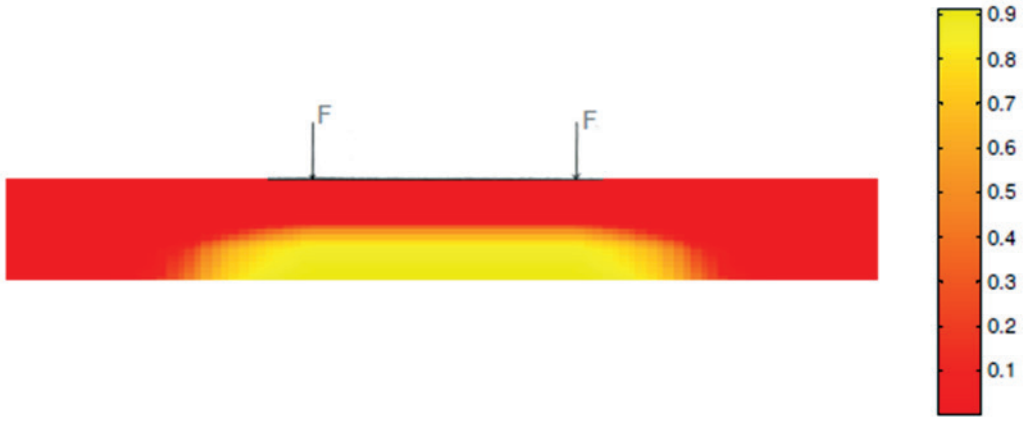

A Numerical evaluation of tensile damage (D_i) with the proposed load of 85.80 kN

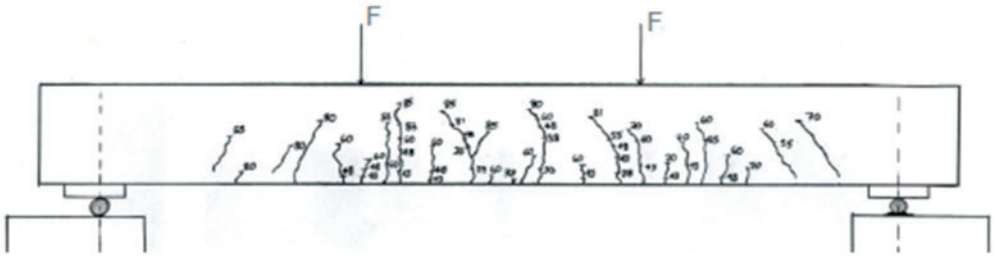

B Cracking map elaborated by Lopes (15) with the 85.80 kN load

Figure 20 shows the numerical and experimental load–displacement curve in the middle span of the V7 beam with a steel fiber content of 0.50%. The numerical responses were obtained using the parameters of the homogenization model from three different prismatic specimen sizes. The names P450, P600, and P300 refer to the span of the prismatic specimens; that is, P450 refers to the 150 × 150 × 500 mm specimen, P600 to the 200 × 200 × 800 mm specimen, and P300 to the 100 × 100 × 400 mm specimen. Analyses were performed in the service load state.

It is possible to note the size effect on the high-level load of the beam. As this paper is concerned with the mechanical behavior in the service load state whose results are in agreement with experimental ones, all analyses were performed with parameters obtained from specimen P600.

The maximum experimental load was 111.8 kN and the estimated service load for the numerical analysis was 44.75 kN. The displacement in the middle span of the beam for the experimental service load was 0.503 mm, whereas the displacement obtained from the numerical analysis was 0.514 mm, presenting an error of 2%.

Table 12 – Steel fiber properties used by Oliveira (17)

Analysed property	Value
Modulus of elasticity (GPa)	200
Tensile resistance (MPa)	1100
Specific weight (kg/m³)	7850
Length (mm)	60
Diameter (mm)	0.75
Aspect ratio (l/d)	80

Table 13 – Mechanical properties of the concrete beams tested by Oliveira (17)

Beam	f_{cm} (MPa)	Modulus of elasticity E_{cm} (GPa)	Poisson ratio (υ)	Fiber percentage (%)
V7	55.27	51.10	0.21	0.50
V8	53.27	45.20	0.18	0.75
V9	62.33	40.67	0.18	1.25

Table 14 – Damage parameters and elastic modulus of concrete without fibers identified from the four-point flexural tests on prismatic specimens of 150 mm × 150 mm × 500 mm

Parameters	Tensile	Compression	$F_{pico, num}$ (kN)	$F_{pico, num} / F_{pico, exp}$
E (MPa)	33700	33700	78.74	1.24%
A	12	0.7	78.74	1.24%
B (Mpa^{-1})	6500	2.5	78.74	1.24%
YO (Mpa)	0.000003	0.004945	78.74	1.24%
β	0.00000295	0.0003	78.74	1.24%

Table 15 – Model parameters for homogenization of La Borderier (4) for concrete with 1.25% fibers – Example III

Fiber volume	$F_{pico, num}$ (kN)	Peak stress – σ_{pic} (MPa)	Yield stress – σ_s (MPa)	Strain fracture – ε_{rupt} (m/m)	$F_{pico, num} / F_{pico, exp}$
1.25%	78.74	430.00	344.00	0.0400	1.24

Table 16 – Model parameters for homogenization of La Borderier (4) for the beam V8 with 0.75% steel fibers by Oliveira (17)

Fiber volume	$F_{pico, num}$ (kN)	Peak stress – σ_{pic} (MPa)	Yield stress – σ_s (MPa)	Strain fracture – ε_{rupt} (m/m)	$F_{pico, num} / F_{pico, exp}$
0.75%	54.31	480.00	384.00	0.040	0.254%

Table 17 – La Borderie (4) parameters for the calibrated curve of the concrete beam V7 with 0.5% fibers

Fiber volume	$F_{pico, num}$ (kN)	Prismatic specimens	Peak stress – σ_{pic} (MPa)	Yield stress – σ_s (MPa)	Strain fracture – ε_{rupt} (m/m)	$F_{pico, num} / F_{pico, exp}$
0.50%	22.89	100 × 100 × 450 mm	675.00	540.00	0.040	0.180%
0.50%	46.84	150 × 150 × 500 mm	615.00	492.00	0.040	1.134%
0.50%	61.17	200 × 200 × 800 mm	430.00	344.00	0.040	0.015%

Table 18 – Longitudinal reinforcement data used in the modeling of beams tested by Oliveira (17)

Beam	Modulus of elasticity (MPa)	Peak stress – σ_{pic} (MPa)	Yield stress – σ_s (MPa)	Strain fracture – ε_{rupt} (m/m)
V7	210000	729	628	1.115
V8	210000	729	628	1.115
V9	210000	790	651	1.013

Figure 21 shows the tension damage distribution near to the load of 50 kN. Even at small load levels, the beam shows high damage values in the middle span due to the small reinforcement rate used in this beam. At that loading level, there is fracture nucleation in the experimental test. The numerical modeling tries to reproduce this phenomenon, evidencing a decrease in strength for a load of 55 kN. However, the numerical modeling shows a recovery of strength and the mechanical behavior of the beam starts to be influenced by the homogenization model. Figure 22 illustrates this phenomenon, presenting a greater increase of the damage in the first layer of the beam in the middle span when the load increases from 50 to 60 kN.

Figure 23 shows the numerical and experimental load–displacement curves for the V8 beam with a fiber content of 0.75%. For

Figure 16 – Numerical curve versus experimental prismatic specimens of V9 beam by Oliveira (17) with 1.25% fibers

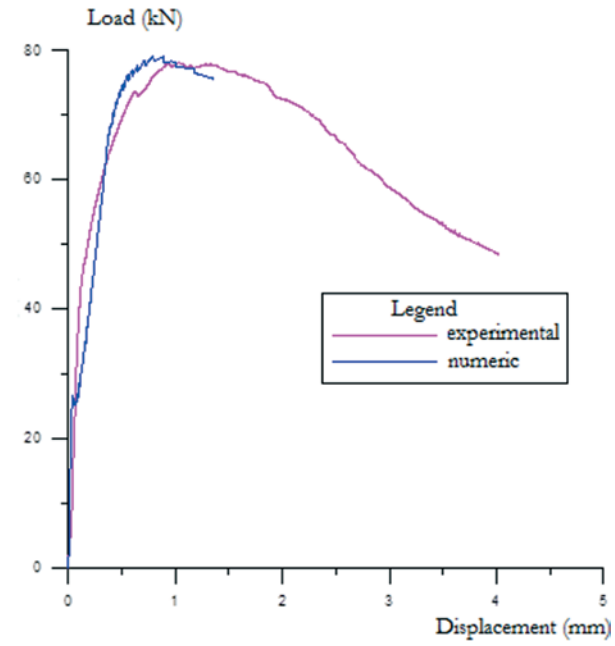

Figure 17 – Numerical curve versus experimental prismatic specimens of V8 beam by Oliveira (17) with 0.75% fibers

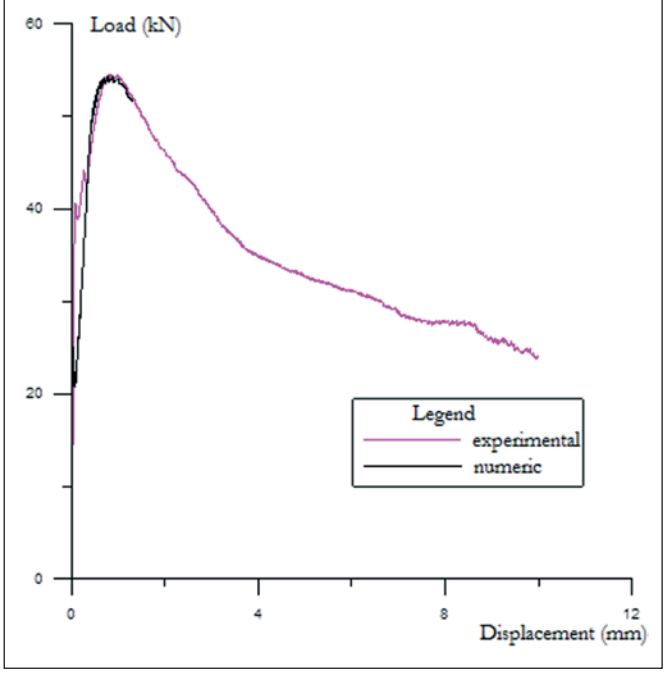

this beam, the numerical analysis does not show results after a load of 80 kN due to the intense damage process. The maximum load applied to this beam was 138.21 kN and a service load equal to 55.29 kN was adopted. For this load, the experimental displacement in the middle span of the beam was 0.730 mm, whereas the numerical analysis achieved a displacement of 1.398 mm, representing an error of 92%. For loads smaller than 53 kN, the damage model presented a smaller error compared to experimental values. For example, an error of just 7% was obtained for a load of 52.11 kN. In this case, the vertical displacement estimated by the Brazilian Standard NBR 6118 [2014] was 0.510 mm, representing a value 23% smaller than the experimental one.

The numerical and experimental load–displacement curves for the V9 beam are shown in Figure 24. The service load for this beam was estimated as 66.48 kN, which corresponds to an experimental displacement of 0.844 mm. The numerical modeling presented a value of 1.56 mm, that is, 87% greater than the experimental value. For small loads, the numerical modeling presents good results when compared to the experimental ones. For example, an error of 17% is presented for a loading of about 58.62 kN. In this case, the vertical displacement estimated by the Brazilian Standard NBR 6118 [2014] was 0.512 mm, which represents a value 30% smaller than the experimental one.

In order to evaluate a possible influence of the steel fiber orientation, the three beams tested by Oliveira [17] were simulated again in order to find new parameters for the homogenization model. In this case, the inverse analysis was performed on the experimental response of the beams and not on the prismatic specimen response. Figures 25 to 27 show the load–displacement curves for the new parameters of La Borderie's model [4], which are shown in Table 19. First of all, there is a better approach for the maximum numerical load to the maximum experimental load. However, a difference between the numerical and experimental responses after the damage localization in the middle of the span is still noted. This divergence tends to decrease with increasing the steel fiber content due to a more distributed cracking along the tested beams. Another important observation is that the parameters of the homogenization model vary with the fiber content, as one would expect from La Borderie's model. However, these parameters show a little variation for fiber contents greater than 0.75%, which approximately represents the critical fiber content for this concrete matrix.

4. Conclusions

First of all, it is important to note that the damage model is capable of dealing with structures in service loading state. It is possible to

Table 19 – Model parameters of homogenization by La Borderier (4) obtained by retro-analysis of the beams tested by Oliveira (17)

Beam	Fiber volume (%)	F_{pico} (kN)	Peak stress – σ_{pic} (MPa)	Yield stress – σ_s (MPa)	Strain fracture – ε_{rupt} (m/m)	$F_{pico, num}$ / $F_{pico, exp}$
V7	0.50	110.21	220.00	187.00	0.020	1.49%
V8	0.75	130.88	240.00	204.00	0.020	5.69%
V9	1.25	170.66	245.00	208.50	0.020	2.09%

observe that in the service loading state (defined in this paper as about 40% of the ultimate loading), the numerical model presented good results compared to experimental tests.

Another factor observed in all examples is the massive process damage in the more tensioned layers even under service loading state. The constitutive model represents the cracking pattern of beams under flexure well. As the cracking process intensifies, it naturally leads to fracture nucleation. Thus, as the loading increases and the cracking process intensifies, it is expected that the damage model will present instabilities and numerical convergence

Figure 18 – Numerical curve versus experimental prismatic specimens of V7 beam by Oliveira (17) with 0.50% fibers

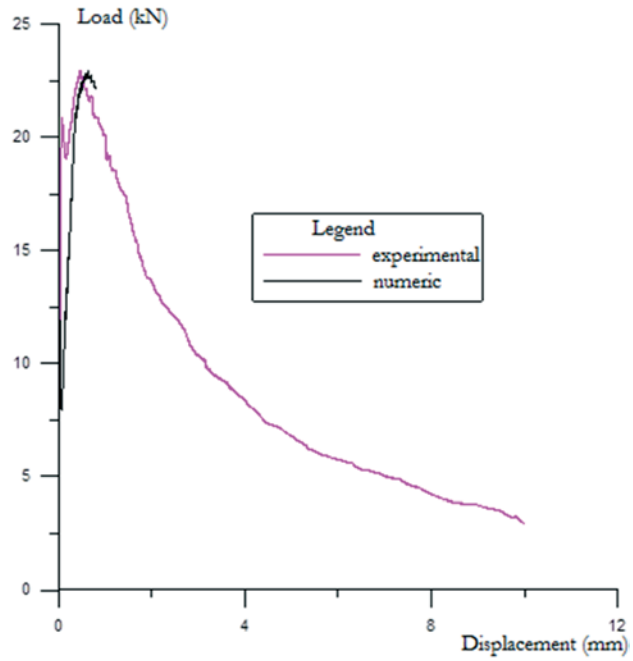

A Prismatic specimens of 100 mm × 100 mm × 450 mm

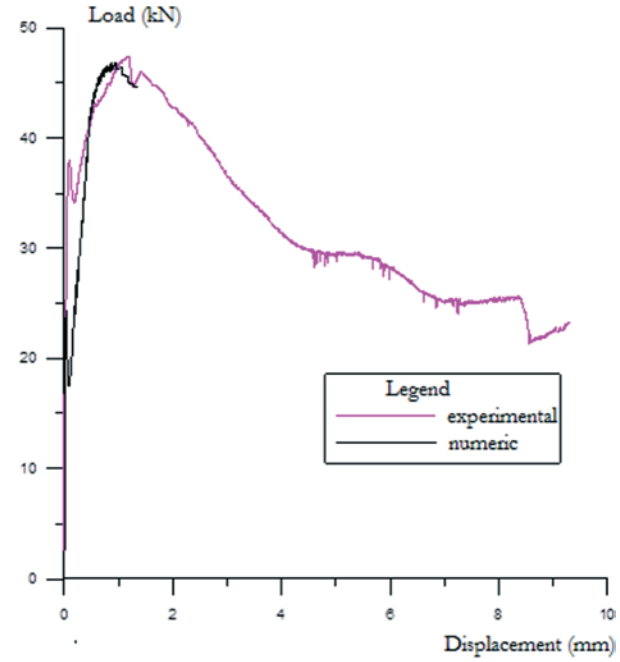

B Prismatic specimens of 150 mm × 150 mm × 500 mm

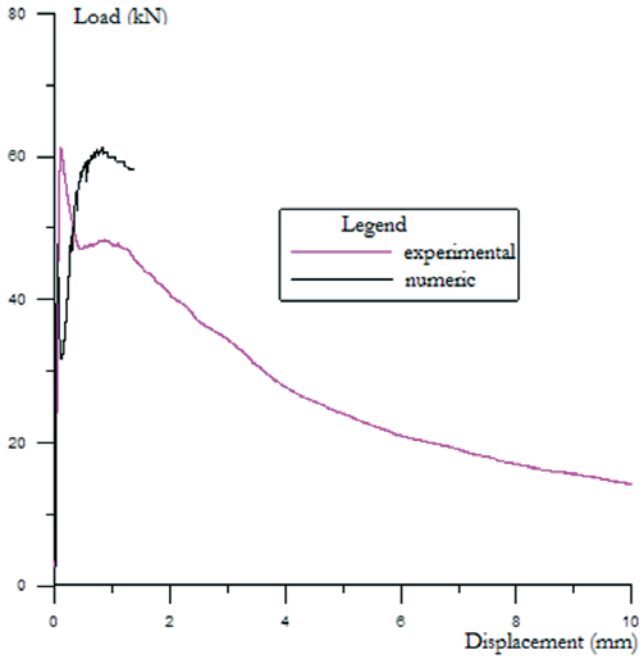

C Prismatic specimens of 200 mm × 200 mm × 800 mm

Figure 19 – Beam numerically tested based on Oliveira's (18) geometry

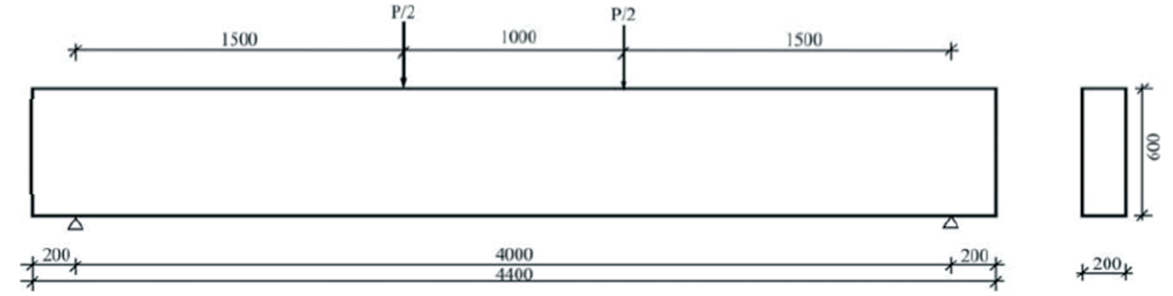

A Beam geometry tested by Oliveira (18)

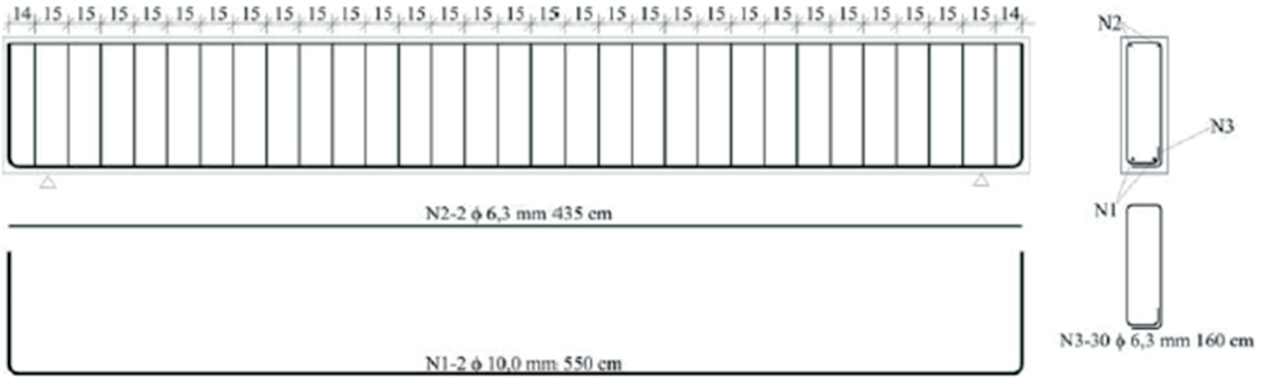

B Beam reinforcement tested by Oliveira (18)

Figure 20 – Numerical and experimental curves of beam V7 of Oliveira (17)

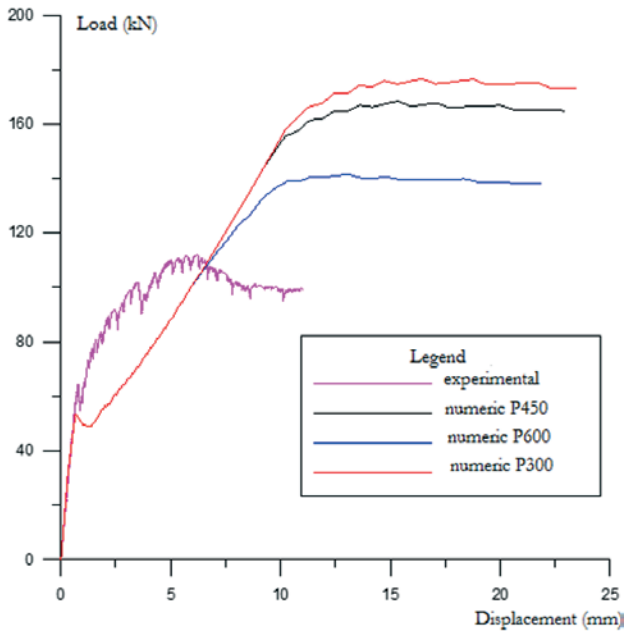

Figure 21 – Damage by tensile (D_t) in beam V7 of Oliveira (17) for a specific strength

A 44.75 kN strength

B 60.00 kN strength

Figure 22 – Comparison of damage in the first layer of beam V7

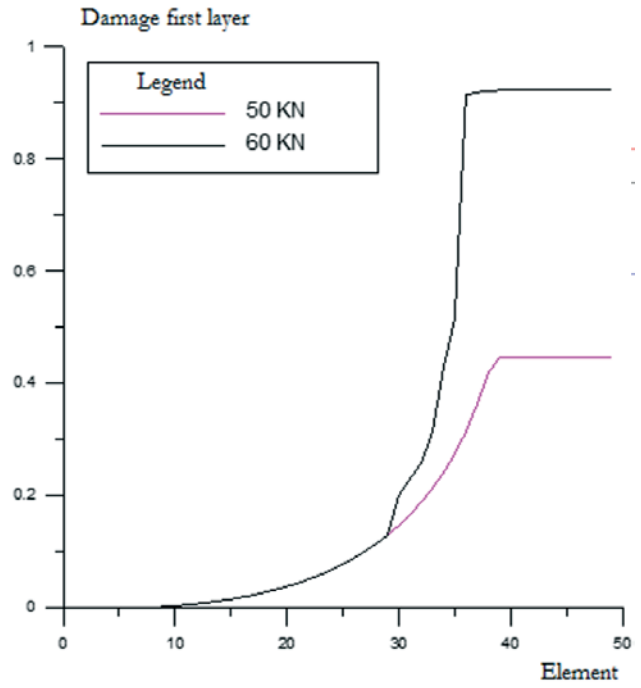

Figure 23 – Load versus numerical and experimental displacement of beam V8 of Oliveira (17)

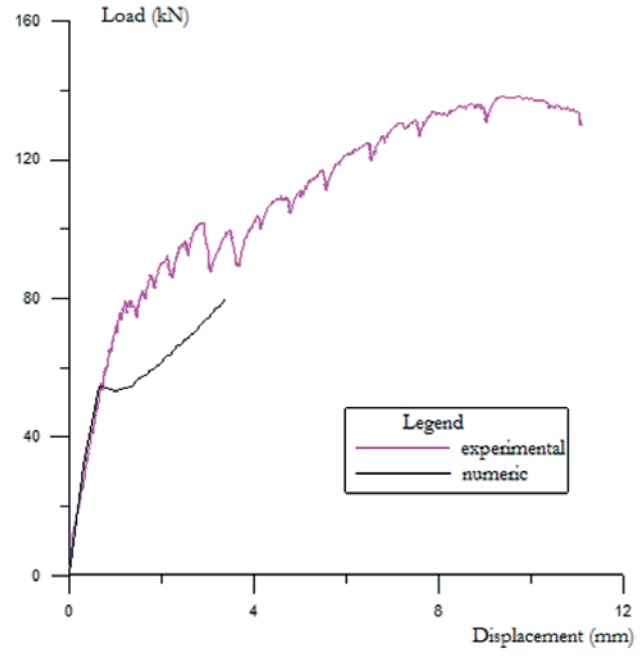

Figure 24 – Load versus numerical and experimental displacement of beam V9 of Oliveira (17)

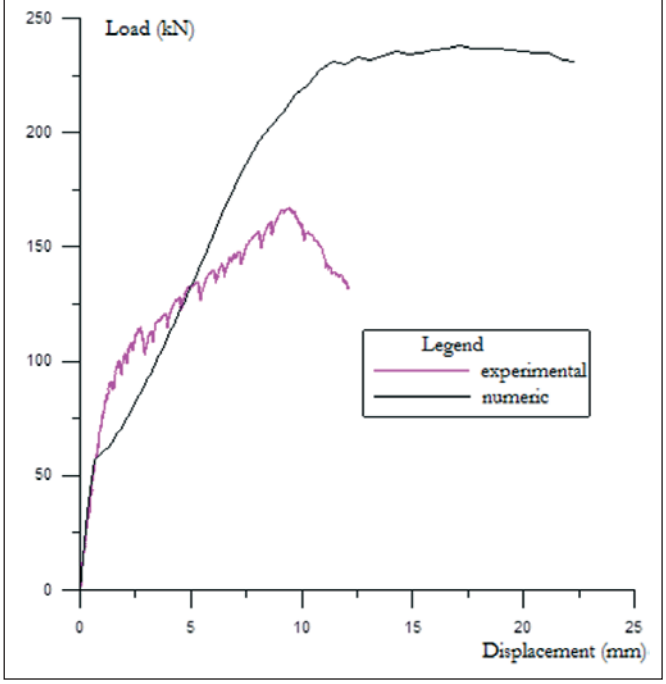

Figure 25 – Parametric identification through beam V7 with 0.5% fibers

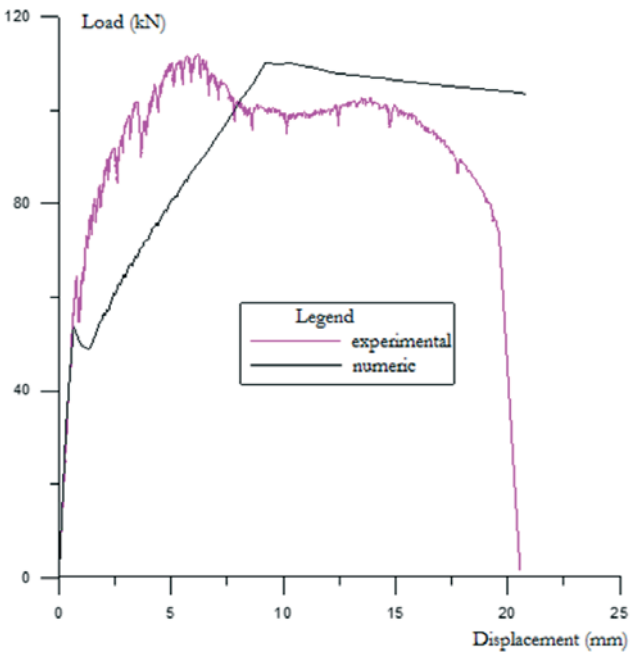

Figure 26 – Parametric identification through beam V8 with 0.75% fibers

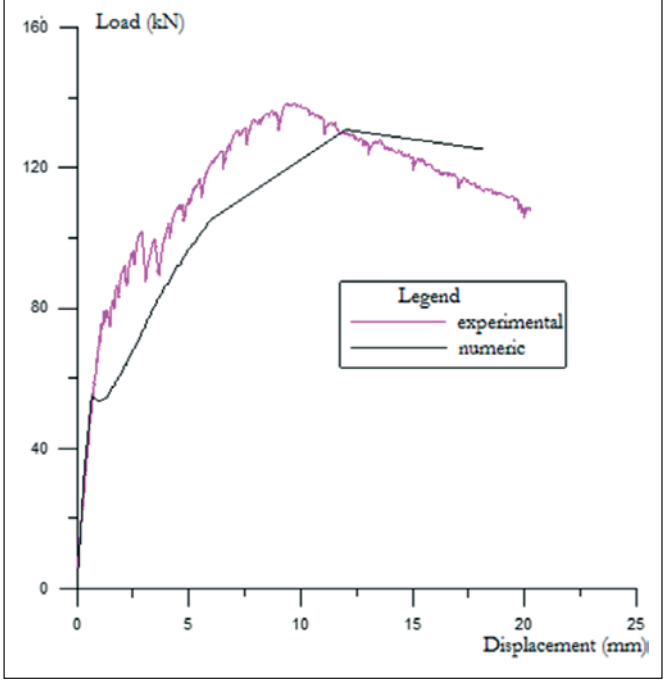

Figure 27 – Parametric identification through beam V9 with 1.25% fibers

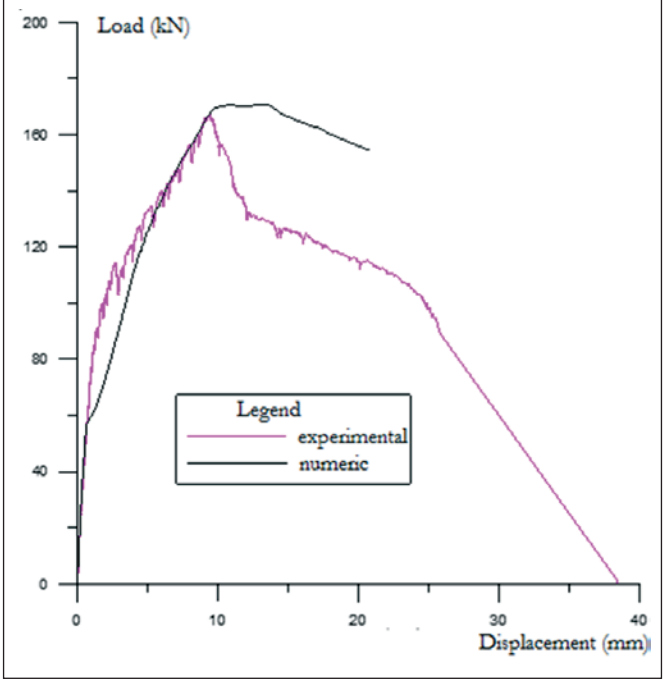

problems. In fact, these problems arise after the service loading state. This feature is more pronounced in concrete prisms with or without low values of fiber content, in which there is nucleation of localized fractures in the absence of reinforcement. Therefore, the damage model cannot capture the effect of strain localization. In future work, the authors intend to propose a two-dimensional modeling coupling a fracture model with the damage model in order to investigate the localization problem described here.

The parametric identification of a constitutive model is one of the most important features involved in computational modeling of structures. It is observed that the responses obtained from beam modeling in the third example are not satisfactory with regard to the softening behavior. In addition, the damage model does not consider the fracture nucleation, another important observation concerns the possible influence of the size effect and the fiber orientation. In both the second and the third example, the parametric identifications were performed in prismatic specimens with dimensions smaller than those of the beams. As the damage model does not take into account those two factors, it may be that the numerical response was affected and the numerical strength was greater than the results obtained from experimental tests. The change of prismatic size of the V7 beam in the third example led to changes of the homogenization parameters and consequently changes in the numerical response of the beam.

The influence of the size effect and fiber orientation can be more pronounced when the parameters of the homogenization model have been obtained from inverse analysis of the beams. In this case, a reduction of the maximum load obtained from numerical modeling, which was nearest to the experimental values, was observed. This suggests that fewer steel fibers were oriented in the longitudinal direction of the beams. The increase in the maximum load of the beams in the third example was not proportional to the increase in fiber content. On the other hand, the parameters obtained from the inverse analysis of prismatic specimens in the second example were adequate to represent the service state of the beam, as well as the maximum experimental load. This feature can be explained by the similarity of the cross-section dimensions of the specimen and the beam in this example.

Finally, it can be concluded that the damage model can be applied in the analysis of steel-fiber-reinforced concrete beams once the numerical responses show good agreement with the experimental results, mainly in service loading state. In a preliminary analysis, if the proposed damage model response is compared with the displacement evaluated from the Brazilian Standard NBR 6118 [2014], the damage model tends to provide values of displacement closer to those observed in the experimental tests. However, this assertion needs to be better investigated in future works.

5. Acknowledgments

Financial support from CAPES Foundation, the Ministry of Education of Brazil, and CNPq (National Council for Scientific and Technological Development) is gratefully acknowledged.

6. References

[1] MATALLAH, M.; LA BORDERIE, C. Inelasticity–damage-based model for numerical modeling of concrete cracking,

Engineering Fracture Mechanics, v. 76, pp. 1087–1108, 2009.

[2] BIELSKI, J.; SKRZYPEK, J. J.; KUNA-CISKAL, H. Implementation of a model of couled elastic-plastic unilateral damage material to finite element code. International Journal of Damage Mechanics, v. 15, pp. 5–39, 2006.

[3] PITUBA, J. J. C.; FERNANDES, G. R.. Anisotropic damage model for concrete. Journal of Engineering Mechanics, v. 137, pp. 610–624, 2011.

[4] LA BORDERIE, C. Phenomenes unilateraux dans un materiau endommageable: modelisation et application a l'analyse de structures en beton. Tese (Doutorado em Engenharia), Universidade de Paris, Paris, 1991, 140 p.

[5] LI, F., LI, Z. Continuum damage mechanics based modeling of fiber reinforced concrete in tension. International Journal of Solid and Structures. Hong Kong, v. 38, p. 777–793, 1999.

[6] LEE, H. K., LIANG, Z. Computational modeling of the response and damage behavior of fiber reinforced cellular concrete. Computers & Structures. USA, v. 82, p. 581–592, 2004.

[7] HAMEED, R., SELLIER, A., TURATSINZE, A., DUPRAT, F. Damage modeling of metallic fiber-reinforced concrete. Engineering Procedia. France, v. 10, p. 1670–1678, 2011.

[8] PASA, V. F. Análise do comportamento de estruturas de concreto reforçado com fibras de aço via método dos elementos finitos. Dissertação (Mestrado em Engenharia de Estruturas), Universidade Federal do Rio Grande do Sul, Porto Alegre, 2007, 130 p.

[9] GUELLO, G. A. Simulação computacional de estruturas de concreto por meio da mecânica do dano. Dissertação (Mestrado em Engenharia de Estruturas), Escola Politécnica de São Paulo, Universidade de São Paulo, São Paulo, 2002, 105 p.

[10] PITUBA, J. J. C. Sobre a formulação de um modelo de dano para concreto. Tese (Doutorado em Engenharia de Estruturas), Escola de Engenharia de São Carlos, Universidade de São Paulo, São Paulo, 2003, 151 p.

[11] COMI, C.; PEREGO, U. A bi-dissipative damage model for concrete with applications to dam engineering. European Congress on Computational Methods in Applied Sciencs and Engineering (ECOMAS 2000), 2000.

[12] RAMTANI, S.; BERTHAUD, Y.; MAZARS, J. Orthotropic behavior of concrete with directional aspects: modeling and experiments. Nuclear Engineering Design, v. 133, pp. 97–111, 1992.

[13] VELASCO, R. V. Concretos auto-adensáveis reforçados com elevadas frações Volumétricas de fibras de aço: propriedades reológicas, Físicas, mecânicas e térmicas. Tese (Doutorado em Ciências em Engenharia Civil), Universidade Federal do Rio de Janeiro, 2008, 349 p.

[14] ABNT – ASSOCIAÇÃO BRASILEIRA DE NORMAS TÉCNICAS. NBR 15530: Fibras de aço para concreto – Especificação. Rio de Janeiro, 2007, 7 p.

[15] LOPES, M. M. Substituição parcial de armadura de flexão por fibras de aço em vigas de concreto. Dissertação (Mestrado em Engenharia Civil), Universidade Federal do Rio de Janeiro, Rio de Janeiro, 2005, 155 p.

[16] PEREIRA JUNIOR, W. M. Análise numérica de estruturas de concreto com fibras utilizando mecânica do dano. Dissertação (Mestrado em Geotecnia, Estruturas e Construção Civil s), Escola de Engenharia Civil da Universidade de Goiás, Universidade Federal de Goiás, Goiânia, 2014, 157 p.

[17] OLIVEIRA, C. A. S. Avaliação da redução de armadura mínima de flexão em vigas de concreto armado com adição de fibras de aço. Dissertação (Mestrado em Engenharia Civil), Universidade Federal de Goiás, Goiânia, 2008, 231 p.

[18] BENTUR, A., MINDESS, S. Fiber Reinforced Cementitious Composites. Elsevier Science, 1990.